




# Mono-, bi-, and tri-metallic Ni-based catalysts for the catalytic hydrotreatment of pyrolysis liquids

Wang Yin<sup>1</sup> · Robbie H. Venderbosch<sup>2</sup> · Songbo He<sup>1</sup> · Maria V. Bykova<sup>3,4</sup> · Sofia A. Khromova<sup>3</sup> · Vadim A. Yakovlev<sup>3</sup> · Hero J. Heeres<sup>1</sup> 

Received: 10 December 2016 / Revised: 10 May 2017 / Accepted: 12 May 2017 / Published online: 3 June 2017  
© The Author(s) 2017. This article is an open access publication

**Abstract** Catalytic hydrotreatment is a promising technology to convert pyrolysis liquids into intermediates with improved properties. Here, we report a catalyst screening study on the catalytic hydrotreatment of pyrolysis liquids using bi- and tri-metallic nickel-based catalysts in a batch autoclave (initial hydrogen pressure of 140 bar, 350 °C, 4 h). The catalysts are characterized by a high nickel metal loading (41 to 57 wt%), promoted by Cu, Pd, Mo, and/or combination thereof, in a SiO<sub>2</sub>, SiO<sub>2</sub>-ZrO<sub>2</sub>, or SiO<sub>2</sub>-Al<sub>2</sub>O<sub>3</sub> matrix. The hydrotreatment results were compared with a benchmark Ru/C catalyst. The results revealed that the monometallic Ni catalyst is the least active and that particularly the use of Mo as the promoter is favored when considering activity and product properties. For Mo promotion, a product oil with improved properties viz. the highest H/C molar ratio and the lowest coking tendency was obtained. A drawback when using Mo as the promoter is the relatively high methane yield, which is close to that for Ru/C. <sup>1</sup>H, <sup>13</sup>C-NMR, heteronuclear single quantum coherence (HSQC), and two-dimensional gas chromatography (GC × GC) of the product oils reveal that representative component classes of the sugar fraction of pyrolysis liquids like

carbonyl compounds (aldehydes and ketones and carbohydrates) are converted to a large extent. The pyrolytic lignin fraction is less reactive, though some degree of hydrocracking is observed.

**Keywords** Pyrolysis liquids · Nickel-based catalysts · Batch autoclave · Hydrogenation

## 1 Introduction

Lignocellulosic biomass is the only sustainable resource containing carbon. It can be transformed into alternatives for fossil-derived crude oil and derivatives [1]. Biomass, however, has a lower energy density compared to fossil-derived liquid products and collection is costly. In addition, lignocellulosic biomass also shows considerable differences in structure and composition. It is thus imperative to develop efficient liquefaction methods to increase the energy density and as such to decrease the costs of transportation [2].

Fast pyrolysis is a very suitable technology to convert solid biomass to mainly liquid products. In the process, hot vapors are generated that are quickly quenched into a liquid product. The condensable liquids are up to 70 wt% based on dry biomass feed and are referred to as pyrolysis liquids (PLs), bio-oils, pyrolysis oils, or bio-crudes [3]. PLs contain high amounts of oxygenated components, e.g., water, acids, alcohols, aldehydes, ketones, sugar monomers, and oligomers as well as lignin monomers and oligomers [3, 4]. The presence of acids is an issue as it leads to corrosion of for instance pipes, valves, and critical parts in diesel engines (e.g., injectors) [5]. More importantly, and partially due to the high oxygen content, the thermal stability of the pyrolysis liquids is limited. Reactive oxygenated compounds, e.g., aldehydes, ketones, and sugars, are considered the main cause of the observed increase in viscosity during storage [6, 7], due to

**Electronic supplementary material** The online version of this article (doi:10.1007/s13399-017-0267-5) contains supplementary material, which is available to authorized users.

✉ Hero J. Heeres  
h.j.heeres@rug.nl

<sup>1</sup> Department of Chemical Engineering, University of Groningen, Nijenborgh 4, 9747 AG Groningen, The Netherlands

<sup>2</sup> Biomass Technology Group BV, Josink Esweg 34, 7545 PN Enschede, The Netherlands

<sup>3</sup> Boreskov Institute of Catalysis, 5, pr. Akad. Lavrentieva, 630090 Novosibirsk, Russia

<sup>4</sup> Novosibirsk State University, 2 str. Pirogova, 630090 Novosibirsk, Russia

polymerization reactions, which take place even at low temperatures [2]. These carbonyl-containing components are also expected to lead to char formation upon processing of PLs [7]. As such, there is an incentive to upgrade PLs and particularly to reduce acidity and to increase the storage stability to broaden the application range. Examples of such upgrading processes are catalytic hydrotreatments [8–10], high-pressure thermal treatments (HPTT) [11], and cracking using zeolites [12].

During the catalytic hydrotreatment, the PLs are subjected to elevated temperatures under relatively high pressures of H<sub>2</sub> in the presence of a suitable catalyst [10, 13–15]. The process severity (temperature, pressure) is of importance to steer product properties (oxygen content, water content, thermal stability). A number of classes of catalysts have been reported for the catalytic hydrotreatment of PLs. Conventional hydrodesulfurization catalysts, e.g., sulfided NiMo and CoMo on  $\gamma$ -Al<sub>2</sub>O<sub>3</sub>, have been tested extensively but, while full deoxygenation is possible [16], catalyst stability appears an issue. Recently, noble metal catalysts, including Ru, Pd, Pt, and Rh, on various supports (Al<sub>2</sub>O<sub>3</sub>, TiO<sub>2</sub>, active carbon, ZrO<sub>2</sub>, etc.) [15, 17], have been introduced that may be less pronounced to deactivation. Ru/C was found to be a superior catalyst compared to the classical hydrotreating catalysts with respect to oil yield (up to 60 wt%) and deoxygenation level (up to 90 wt%) [15]. Ru/C was used in extensive studies and it was shown that an initial low temperature stage (<200 °C) is advantageous to reduce char formation and to avoid rapid blockage of the reactor. Based on these findings, a reaction network was proposed [2], including hydrogenation, hydrocracking/hydrodeoxygenation, and repolymerization reactions. It was shown that, particularly in the initial low temperature stage of the reaction, reactive aldehydes and ketones (including carbohydrates) are converted to alcohols. A competing reaction is the thermal repolymerization of such molecules to oligomers and finally to char. As such, it is of prime importance to identify catalysts that are particularly active in this initial stage of the reaction.

To reduce catalysts cost, which is particularly relevant when (irreversible) catalyst deactivation plays a role, there is a clear incentive to use non-noble metal-based catalyst formulations. Examples are non-sulfided Co-Mo-B and Ni-Mo-B catalysts and transition metal (Ni, Fe, Mo, Co, W) phosphides supported on silica, which have been tested for pyrolysis liquid model compounds. Hydrodeoxygenation of phenol and cyclopentanone using such catalysts yielded up to 93% of fully deoxygenated products [18–21]. The rate of hydrodeoxygenation of guaiacol was shown to follow the order: Ni<sub>2</sub>P > Co<sub>2</sub>P > Fe<sub>2</sub>P, WP, MoP [22]. The positive effect of B and P additives on catalyst activity was observed in both cases, but again, catalysts deactivate due to the loss of active components during the reaction.

Recently, we reported the use of bi-metallic Ni-Cu catalysts supported on  $\delta$ -Al<sub>2</sub>O<sub>3</sub>, CeO<sub>2</sub>-ZrO<sub>2</sub>, ZrO<sub>2</sub>, SiO<sub>2</sub>, TiO<sub>2</sub>, rice

husk carbon, and Sibunit for the catalytic hydrotreatment of PLs [23]. Though product oils with improved properties were obtained, char was still formed, indicating that the hydrogenation rate at low temperatures is relatively slow. Subsequently, a bi-metallic Ni-Cu catalyst [24] was tested in a packed bed set-up for the catalytic hydrotreatment of pyrolysis liquids. This catalyst is characterized by a high nickel loading (57.9 wt%, 7.0 wt% of Cu and 35.1 wt% of SiO<sub>2</sub>). The catalyst showed good activity at low temperature compared to the benchmark Ru/C as well as the supported NiCu catalysts with a lower Ni loading and polymerization was suppressed to a large extent.

In a later study, we reported the synthesis and application of Ni-based catalysts promoted by Cu and Pd for the catalytic hydrotreatment of PLs at 350 °C in a batch autoclave [25]. Products with a high H/C ratio and low coking tendency were observed. Ni-based catalysts with Pd as the promoter were shown to be favored compared to Cu, but, as Pd is much more expensive than Cu, the potential of such Pd promoted catalysts may be limited.

Motivated by the performance of Pd- and Cu-doped Ni-based catalysts, we here report a catalyst screening study with Ni-based catalysts promoted particularly by Mo for the catalytic hydrotreatment of PLs (350 °C, 140 bar H<sub>2</sub>) in a batch autoclave. These conditions were selected based on earlier catalyst screening studies by our group [23, 25–28]. Both bi- and tri-metallic catalyst Ni-based catalysts were prepared and tested with Mo, Cu, and Pd as promoters. The use of Ni-based, Mo-promoted catalysts with a high Ni content prepared using a sol-gel technique for the catalytic hydrotreatment of pyrolysis liquids has not been reported in the literature and is a novelty of this paper. In addition, performance was compared to the benchmark noble metal Ru/C catalyst. The product oils were analyzed by various techniques such as elemental analysis, gel permeation chromatography (GPC), thermogravimetric analysis (TGA), <sup>1</sup>H, <sup>13</sup>C-NMR, heteronuclear single quantum coherence (HSQC), and two-dimensional gas chromatography (GC × GC) analysis to determine relevant product properties as well as to gain insights in the molecular transformations occurring during the catalytic hydrotreatment process.

## 2 Experimental section

### 2.1 Materials

The pine wood-derived pyrolysis liquid feed was supplied by the Biomass Technology Group (BTG, Enschede, The Netherlands). Relevant properties of the PLs were determined, and the results are given in Table 1.

Hydrogen, nitrogen, and helium were obtained from Linde and were all of analytical grade (>99.99%). A reference gas containing H<sub>2</sub>, CH<sub>4</sub>, ethylene, ethane, propylene, propane, CO,

**Table 1** Relevant properties of the PL used in this study

Water content (wt%)	22.5
Elemental composition on dry basis (wt%)	
C	64.0
H	6.8
O (by difference)	29.2
N	<0.01
H/C, molar, dry	1.28
O/C, molar, dry	0.34

and CO<sub>2</sub> with known composition for gas phase calibration was purchased from Westfalen AG, Münster, Germany. Ru/C (5 wt% metal loading) was purchased from KaiDa Technology Limited, UK. Tetrahydrofuran (THF, anhydrous), di-*n*-butyl ether (DBE, anhydrous, 99.3%), dimethyl sulfoxide-d<sub>6</sub> (99.6 atom % D), chloroform-d<sub>1</sub> (99.96 atom % D), and CaCl<sub>2</sub> (anhydrous, ≥93.0%) were purchased from Sigma-Aldrich and used without further purification, and levoglucosan was supplied from Carbosynth, UK and used as received.

## 2.2 Catalyst synthesis and composition

The catalysts were prepared using a sol-gel method according to a procedure reported by Bykova et al. [29–32]. The amounts of active metals, supports, and activation parameters are summarized in Table 2. The catalysts were crushed and sieved, and the fraction between 25 and 75 μm was used for the hydrotreatment reactions.

## 2.3 Experimental procedures

### 2.3.1 Catalytic hydrotreatment of pyrolysis liquids in a batch autoclave

Catalysts screening experiments were performed in a 100-ml Parr autoclave equipped with an overhead stirrer. Prior to the experiment, the reactor was charged with 1.25 g of catalyst (5 wt% with respect to pyrolysis liquids feed). Subsequently,

the reactor was pressurized with 100 bar of N<sub>2</sub> to check for leakage. The catalyst was then pre-reduced using 20–30 bar H<sub>2</sub> at the temperature given in Table 2 for 1 h. Subsequently, the reactor was cooled to room temperature and 25.0 g of the PL was injected to the reactor from a feed vessel using pressurized nitrogen gas. Then, the reactor was flushed three times with 10 bar of hydrogen to remove air and was subsequently pressurized to 140 bar at room temperature. Finally, the reactor was heated to 350 °C with a heating rate of around 10 °C/min at a stirring speed of 1400 rpm. The reaction was allowed to proceed at 350 °C for 4 h. The reaction was carried out in a batch mode both for the gas and liquid phase and consumed hydrogen was not replenished. Then, the reactor was cooled to ambient temperature and the pressure in the reactor was recorded for mass balance calculations, the reactor was vented, and the gas phase was collected in a 3-L gas bag. The reactor content (liquids and spent catalyst) was collected and transferred to a centrifuge tube and weighed. The liquid phases (water and product oil) were separated by centrifugation (4500 rpm, 30 min) and both phases were collected and weighed. The reactor was thoroughly rinsed with acetone. The acetone phase was evaporated in air, and the resulting product was weighted and added to the organic phase and used as input for the mass balance calculations. The remaining solid residue was combined with the solid residue in the centrifuge tube and filtered over a paper filter, washed with acetone, and dried at 100 °C till constant weight. The amount of char is defined as the amount of solid residue minus the original catalyst intake. The amount of gas phase after reaction was determined by the pressure difference in the reactor before and after reaction at room temperature using the ideal gas law, assuming that the volume of the gas hold-up in the reactor before and after reaction was constant. A detailed procedure for the latter is given in previous studies [17, 27].

### 2.3.2 Product analysis

**GC-TCD** The composition of the gas phase after reaction was determined by GC-thermal conductivity detector (TCD). A

**Table 2** Summary of relevant properties of the catalysts used in this study

Code	Metal loading, wt%				Support, wt%			Reduction temperature, °C
	Ni	Cu	Mo	Pd	SiO <sub>2</sub>	Al <sub>2</sub> O <sub>3</sub>	ZrO <sub>2</sub>	
Ni monometallic	49	–	–	–	16.6	–	21	350
Ni-Cu	46	5	–	–	25	–	10.7	350
Ni-Pd	57	–	–	0.7	26	–	–	350
Ni-Pd-Cu	54	8.2	–	0.7	21	–	–	350
Ni-Mo-Cu	38	3.8	5.9	–	10.8	24	–	400
Ni-Mo	41	–	7.4	–	13.3	24	–	400

Oxidized form. Reduction time of the catalysts was 1 h

Hewlett-Packard 5890 Series II GC equipped with a CP Poraplot Q  $\text{Al}_2\text{O}_3/\text{Na}_2\text{SO}_4$  column (50 m  $\times$  0.5 mm, film thickness 10  $\mu\text{m}$ ) and a CP-molsieve (5 Å) column (25 m  $\times$  0.53 mm, film thickness 50  $\mu\text{m}$ ) was used. The injector temperature was set at 150 °C, the detector temperature at 90 °C. The oven temperature was kept at 40 °C for 2 min, then heated up to 90 °C at 20 °C/min and kept at this temperature for 2 min. Helium was used as the carrier gas. The columns were flushed for 30 s with (reference and sample) gas before starting the measurement. A reference gas containing  $\text{H}_2$ ,  $\text{CH}_4$ ,  $\text{CO}$ ,  $\text{CO}_2$ , ethylene, ethane, propylene, and propane with known composition was used for peak identification and quantification.

**Elemental analysis** The elemental compositions of the PL feed and product oils were analyzed by elemental analysis using a EuroVector EA3400 Series CHNS-O with acetanilide as the reference. The oxygen content was determined by difference. All analyses were carried out at least in duplicate and the average value is reported.

**Water content** The water content of the PL feed and product oils were determined using a Karl-Fischer (Metrohm 702 SM Titrino) titration. About 0.01 g of sample was introduced to an isolated glass chamber containing Hydranal solvent (Riedel de Haen) by a 1-ml syringe. The titration was carried out using Hydranal titrant 5 (Riedel de Haen). Milli-Q water was used for calibration. All analyses were carried out at least in duplicate and the average value is reported.

**Gel permeation chromatography** GPC analyses of the PL feed and product oils were performed using an Agilent HPLC 1100 system equipped with a refractive index detector. Three columns (mixed type E, length 300 mm, i.d. 7.5 mm) in series were used. Polystyrene was used as a calibration standard. Before analysis, 0.05 g of the organic phase was dissolved in 5 ml of THF (10 mg/ml) together with two drops of toluene (flow marker) and filtered (pore size 0.2  $\mu\text{m}$ ) before injection.

**Thermogravimetric analysis** TGA data of the PL feed and product oils were obtained using a TGA 7 from PerkinElmer. The samples were heated in a nitrogen atmosphere with a heating rate 10 °C/min between 20 and 900 °C.

**Gas chromatography/mass spectrometry** Gas chromatography/mass spectrometry (GC-MS) analyses of the liquid products were performed on a Hewlett-Packard 5890 gas chromatograph equipped with a quadrupole Hewlett-Packard 6890 MSD selective detector and a 30-m  $\times$  0.25-mm, i.d. and 0.25- $\mu\text{m}$  film sol-gel capillary column. The injector temperature was set at 250 °C. The oven temperature was kept at 40 °C for 5 min, then increased to 250 °C at a rate of 3 °C/min, and then held at 250 °C for 10 min. Di-*n*-

butyl ether was used as an internal standard for quantification of relevant components in the PLs and products.

**Two-dimensional gas chromatography** GC  $\times$  GC-FID analysis was performed on product oils and the PL feed with a trace GC  $\times$  GC from Interscience equipped with a cryogenic trap system and two columns: a 30-m  $\times$  0.25-mm i.d. and a 0.25- $\mu\text{m}$  film of the RTX-1701 capillary column connected by using a melt fit to a 120-cm  $\times$  0.15-mm i.d. and a 0.15- $\mu\text{m}$  film Rxi-5Sil MS column. An FID detector was used. A dual jet modulator was applied using carbon dioxide to trap the samples. Helium was used as the carrier gas (continuous flow 0.6 ml min<sup>-1</sup>). The injector temperature and FID temperature were set at 250 °C. The oven temperature was maintained at 40 °C for 5 min then heated up to 250 °C at a rate of 3 °C min<sup>-1</sup>. The pressure was set at 70 kPa at 40 °C. The modulation time was 6 s. For GC  $\times$  GC-FID and GC-MS-FID analyses, the samples were diluted with THF and 500 ppm di-*n*-butyl ether (DBE) was added as an internal standard. Detailed procedures regarding calibration and quantification are described in previous studies [33–35].

**<sup>1</sup>H-, <sup>13</sup>C-NMR** For <sup>1</sup>H-NMR, around 10 mg of the PL feed or the product oil was dissolved in 1.0 g of  $\text{CDCl}_3$ . The sample was dried by passing it over a short column containing  $\text{CaCl}_2$ . For <sup>13</sup>C-NMR, 0.5 g of sample was dissolved in 0.5 g of  $\text{DMSO-d}_6$ . The NMR spectra were recorded on a Varian AS400 spectrometer.

**Heteronuclear single quantum coherence NMR** NMR spectra were acquired at 25 °C using an Agilent 400-MHz spectrometer. Approximately 0.5 g of sample was dissolved in 0.5 g of  $\text{DMSO-d}_6$ . <sup>1</sup>H-<sup>13</sup>C HSQC spectra were acquired using a standard pulse sequence with a spectral width of 160 ppm, 16 scans, and 256 increments in the F1 dimension. The data were processed using the MestReNova software.

## 2.4 Catalyst characterization

$\text{NH}_3$ -TPD experiments were performed on Micromeritics AutoChem II 2920. The samples were reduced under  $\text{H}_2$  at 400 °C for 1 h and then purged by He at 500 °C for 1 h. After cooling to 100 °C,  $\text{NH}_3$  was introduced by continuously flowing 1%  $\text{NH}_3/\text{He}$  to samples for 1 h. The desorption of  $\text{NH}_3$  was recorded by TCD with the temperature ramp of 10 °C/min up to 500 °C.

**Temperature programmed reduction** Catalyst samples (0.1 g) were placed in a U-tube quartz reactor and heated under reductive atmosphere (10 vol.% of  $\text{H}_2$  in Ar at a flow rate of 30 ml/min) with a constant heating rate of 8 °C/min up to 800–900 °C. The hydrogen concentration in the outlet stream during the reduction was measured using a TCD.

**Powder X-ray diffraction** Powder X-ray diffraction (XRD) patterns were recorded using a D8 Advance (Bruker, Germany) powder diffractometer in a step scan mode (2 of 0.05°) and accumulation time of 5 s at each point. XRD studies were performed using monochromatic CuK $\alpha$  radiation ( $\lambda = 1.5418 \text{ \AA}$ ) and Lynexeye (1D) linear detector.

The catalysts were studied in initial oxidized form and after reductive treatment in situ in a high temperature chamber XRK-900 (Anton Paar, Austria). In the latter case, samples were heated in a flow of 100% H<sub>2</sub> (30 cm<sup>3</sup>/min) at a rate of 12 °C/min up to the temperature used for catalyst activation prior to the hydrotreatment experiments (350 °C for Ni/SiO<sub>2</sub>-ZrO<sub>2</sub> and Ni-Cu/SiO<sub>2</sub>-ZrO<sub>2</sub> and 400 °C for Ni-Mo/SiO<sub>2</sub>-Al<sub>2</sub>O<sub>3</sub>, see details in Section 2.2). Thereafter, the samples were cooled down to room temperature under continuous H<sub>2</sub> flow, and XRD patterns were recorded.

**High resolution transmission electron microscopy** High resolution transmission electron microscope (HRTEM) images were obtained using a JEM-2010 (JEOL Ltd., Japan, lattice-fringe resolution 0.14 nm) and JEM-2200FS (JEOL Ltd., Japan, lattice-fringe resolution 0.1 nm) electron microscopes operated at an accelerating voltage of 200 kV. The scanning transmission electron microscopy with high angle annular dark field (STEM HAADF) and bright field HRTEM (BF/HRTEM) modes were employed. Local energy-dispersive X-ray analysis (EDXA) was carried out using an EDX spectrometer (EDAX Inc.) fitted with a Si (Li) detector with a resolution of 130 eV. The samples for the HRTEM study were prepared on holey carbon film mounted on an aluminum grid.

## 2.5 Definitions

The hydrogen consumption during reaction was calculated according to a method reported in previous studies from our group and quantified using Eq. (1) [17, 27]. The hydrogen consumption corrected for methane formation was calculated using Eq. (2). Here, it is assumed that all the bound hydrogen in methane is derived from the hydrogen feed.

$$\text{H}_2 \text{ consumption} = \frac{n_{\text{H}_2, \text{initial}} - n_{\text{H}_2, \text{final}}}{m_{\text{PL}, \text{initial}}} \cdot 22.4 \quad (1)$$

$$\begin{aligned} \text{H}_2 \text{ consumption corrected for methane} \\ = \text{H}_2 \text{ consumption} - (2 \cdot n_{\text{methane}} \cdot 22.4) \end{aligned} \quad (2)$$

where the H<sub>2</sub> consumption is the hydrogen uptake (in NL per kg feed),  $n_{\text{H}_2, \text{initial}}$  is the initial amount of hydrogen (in moles) in the reactor,  $n_{\text{H}_2, \text{final}}$  is the amount of hydrogen (in moles) in the reactor after the reaction,  $m_{\text{PL}, \text{initial}}$  is the mass of the pyrolytic liquid fed to the reactor,  $n_{\text{methane}}$  is the amount of methane formed (in moles) in the reactor, and 22.4 is the

standard volume of 1 mol of an ideal gas at standard temperature and pressure.

## 3 Results and discussions

### 3.1 Catalyst characterization

Three representative catalysts including the monometallic Ni catalyst and the bi-metallic Ni-Cu and Ni-Mo catalysts were characterized using temperature programmed reduction (TPR), XRD, TEM, and ammonia-TPD to determine relevant catalyst properties to be used as input for catalyst structure–performance relations.

#### 3.1.1 Temperature programmed reduction

TPR profiles for the catalysts are presented in Fig. 1.

For the monometallic Ni catalyst, hydrogen consumption started at about 340 °C. Two reduction regions are present, one at 340–500 °C and at 500–700 °C. The lower temperature region is attributed to reduction of well-crystallized NiO species, whereas at higher temperatures, reduction of oxidized Ni species with strong interactions with the silica matrix takes place [29, 36, 37].

For the bi-metallic Ni-Cu catalyst, the TPR profile is shifted towards lower temperatures. Again, two main peaks are visible. The lower reduction peak starting at 250 °C (Fig. 1, Ni-Cu/SiO<sub>2</sub>-ZrO<sub>2</sub>) with a maximum at about 330 °C corresponds to reduction of Cu(II) into metallic Cu(0) [25, 38] and reduction of a considerable part of the oxidized Ni species [25, 39]. A second broad peak extending up to 700 °C is associated with hardly reducible nickel silicates.

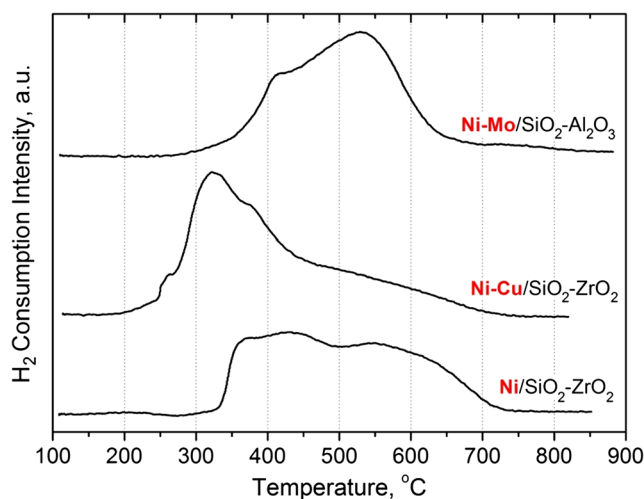


**Fig. 1** Temperature programmed reduction profiles of representative catalysts

For the Ni-Mo/SiO<sub>2</sub>-Al<sub>2</sub>O<sub>3</sub> catalyst, a dominant hydrogen consumption peak centered at 550 °C is visible, which is typical for Mo-containing Ni-based sol-gel catalysts [30]. This peak is associated with reduction of Mo<sup>6+</sup> into Mo<sup>4+</sup> and then to Mo<sup>0</sup>, together with reduction of Ni<sup>2+</sup> to Ni<sup>0</sup>. The small peak at around 410 °C on the left shoulder of the dominant peak is ascribed to the reduction of weakly bound well-crystallized NiO species.

### 3.1.2 X-ray diffraction

X-ray diffraction studies were performed for the catalysts in the initial oxidized state as well as in the reduced form by an in situ reduction in the diffractometer chamber at the conditions specified in Section 2.4. XRD patterns of oxidized Ni/SiO<sub>2</sub>-ZrO<sub>2</sub> (Fig. 2) reveal reflections at 37°, 43°, and 63°, attributed to a NiO phase [PDF no. 471049]. The intensities and positions of these reflections are somewhat different from the reference data and are associated with the formation of silicate-like structures. The formation of such species has been observed previously for related Ni-based catalysts prepared using a sol-gel technique [29, 36, 40]. Of interest is the shape of the NiO peaks, which are sharp at the top but considerably broadened at the base (Fig. 2, Ni/SiO<sub>2</sub>-ZrO<sub>2</sub>, black curve). This is most likely due to a bimodal size distribution of the NiO particles in the catalyst. Thus, the fresh sample very likely contains highly dispersed NiO species responsible for a broadening of XRD reflections, while particles of larger sizes account for the sharp tops of these peaks. In the 2θ range of 30–40°, a halo is visible, which corresponds to amorphous ZrO<sub>2</sub>, in line with literature data [25]. In situ reduction of the catalyst at 350 °C results in the formation of reflections of metallic Ni with a concomitant reduction in the relative intensity of NiO species. The retention of oxide species in the reduced catalyst evidences its incomplete reduction under the selected experimental conditions. This observation is in good agreement with the TPR data (Fig. 1) indicating prolonged hydrogen consumption up to 700 °C for the monometallic one.

The XRD pattern for the Ni-Cu catalyst resembles that of the monometallic one (Fig. 2); however, a number of additional observations can be made. First of all, the XRD pattern after in situ reduction at 350 °C clearly indicates that mostly the larger NiO particles are reduced into metallic Ni species, whereas the highly dispersed NiO particles remain preserved in the catalyst structure probably due to stronger interaction with the silica matrix. Moreover, a higher amount of reduced Ni species is observed, which is associated with the presence of Cu [25]. The formation of Ni<sub>x</sub>Cu<sub>1-x</sub> solid solutions in the Ni-Cu catalyst is confirmed by a higher lattice parameter of the metallic Ni phase (Table 3) [29, 36].

For the Ni-Mo/SiO<sub>2</sub>-Al<sub>2</sub>O<sub>3</sub> in the oxidized form, reflections corresponding to NiO phases are present (Fig. 2). In contrast to other catalysts in the series (Ni monometallic and Ni-Cu), a bimodal distribution of NiO particles is not observed. In addition, the NiO diffraction peaks are broadened, indicative for the

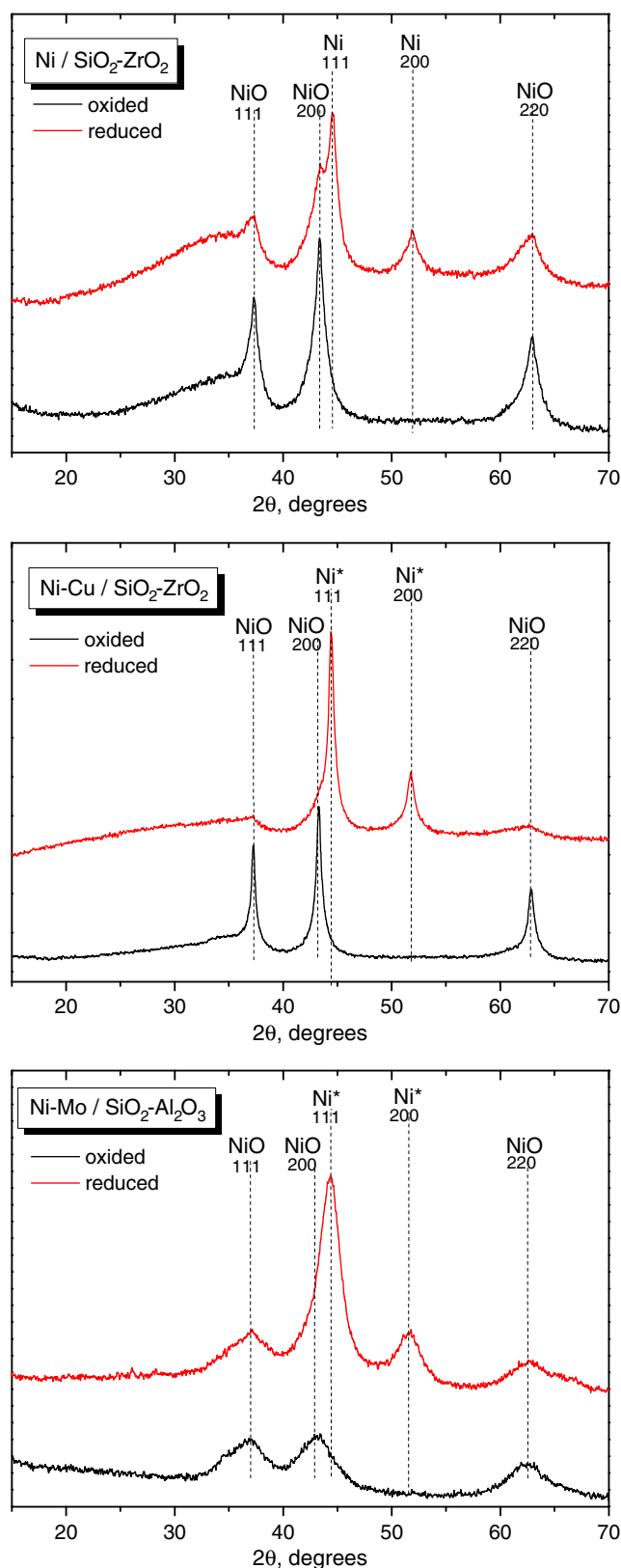


**Fig. 2** XRD patterns of catalysts in their oxidized state (black curve) and after in situ reduction in the diffractometer chamber (red curve). Ni\* represent Ni-based solid solutions

**Table 3** X-ray diffraction data for oxidized and in situ reduced catalysts

Catalyst	State	Phase composition <sup>a</sup>	CSD size (Å)	Lattice parameter for metallic Ni (Å) <sup>c</sup>
Ni/SiO <sub>2</sub> -ZrO <sub>2</sub>	Ox	NiO (100%)	110	3.523
	Red-350 °C	halo <sup>b</sup>		
		Ni (40%)	110	
Ni-Cu/SiO <sub>2</sub> -ZrO <sub>2</sub>	Ox	NiO (100%)	250	3.532
	Red-350 °C	halo <sup>b</sup>		
		Ni* (70%)	180	
		NiO (30%)	65	
Ni-Mo/SiO <sub>2</sub> -Al <sub>2</sub> O <sub>3</sub>	Ox	NiO (100%)	25	3.534
	Red-400 °C	halo <sup>b</sup>		
		Ni* (30%)	50	
		NiO (70%)	25	
		Al <sub>2</sub> O <sub>3</sub>		

<sup>a</sup> Percentages in brackets are determined by the Rietveld method [42] and represent the weight contents of Ni species in the catalyst

<sup>b</sup> halo attributed to amorphous ZrO<sub>2</sub> [25]

<sup>c</sup> Lattice parameters calculated by the Rietveld method [42]

presence of only highly dispersed species. After reduction, the XRD pattern reveals reflections of metallic Ni (Ni\*) and residual NiO. As for the bi-metallic Ni-Cu catalyst, the reflections of metallic nickel are somewhat shifted towards lower  $2\theta$  angles in comparison to the monometallic Ni catalyst and literature data [PDF no. 040850], which is associated with the formation of Ni-Mo solid solutions [30].

Table 3 summarizes the XRD data for the oxidized and reduced catalysts, including phase compositions, the mean sizes of the coherent-scattering domain (CSD) of the Ni-containing species as calculated using the Scherrer equation [41], and lattice parameters for metallic Ni particles. For in situ reduced catalysts, the amounts of Ni-containing species (wt%) were estimated by the Rietveld method [42]. These data show that the reduction extent of catalysts decreases in the order Ni-Cu > Ni > Ni-Mo, in good agreement with the TPR data (Fig. 1). The reduction of both Ni and Ni-Cu samples results in a decrease in the NiO CSD sizes (based on the 111 reflection), indicating that particles of larger sizes are more easily reduced. For the Ni-Mo catalyst, the NiO CSD size does not change after reduction. This is additional evidence that only highly dispersed NiO particles are present in this catalyst.

Of interest is the difference in the mean sizes (CSD) of the metallic Ni species (Ni\*), which is by far the lowest for the bi-metallic Ni-Mo catalyst (50 Å, compared to 180 Å for the Ni-Cu catalyst and 110 Å for the monometallic catalyst). A number of studies have discussed the effects of Ni nanoparticle size on catalytic activity for hydrogenation/hydrodeoxygenation/hydrogenolysis reactions with Ni-based catalysts. For instance, Mortensen et al. [43] reported the hydrodeoxygenation of phenol using Ni/SiO<sub>2</sub> catalysts with Ni nanoparticle sizes ranging from 5

to 22 nm. A strong particle size effect was observed, with intermediate Ni-particle sizes needed for optimal hydrodeoxygenation of phenol. These findings indicate that the reaction is structure sensitive. He et al. [44] studied the catalytic hydrogenolysis of C–O bond in 2-phenylethylphenyl ether ( $\beta$ -O-4), a lignin model component, in water using Ni/SiO<sub>2</sub> catalysts with Ni nanoparticle sizes ranging from 4.5 to 8 nm. The highest activity for C–O bond cleavage was achieved for Ni species with an intermediate Ni nanoparticle size (5.9 nm), again a strong indication for structure sensitivity.

As such, there is a possibility that the catalytic hydrotreatment reaction of PLs is structure sensitive. Surface sites of different configuration (e.g., ensembles of surface atoms), of which the concentration is a function of particle size and shape, then contribute differently to the observed, averaged reaction rate. Detailed overviews on structure sensitive (hydrogenation) reactions are given by Murzin and van Santen et al. [45, 46].

However, our dataset is too limited to draw definite conclusions regarding the optimal Ni\* nanoparticle size for the catalytic hydrotreatment reactions reported here. In addition, many different reactions involving a large amount of individual components occur during the catalytic hydrotreatment of PLs. As such, model component studies with an extended set of Ni-based catalysts will be required to gain insights in the structure sensitivity of the hydrotreatment reaction, which are beyond the scope of the current paper.

### 3.1.3 High resolution transmission electron microscopy

TEM micrographs were recorded for the reduced bi-metallic catalysts (Fig. 3). The morphology of the monometallic Ni/

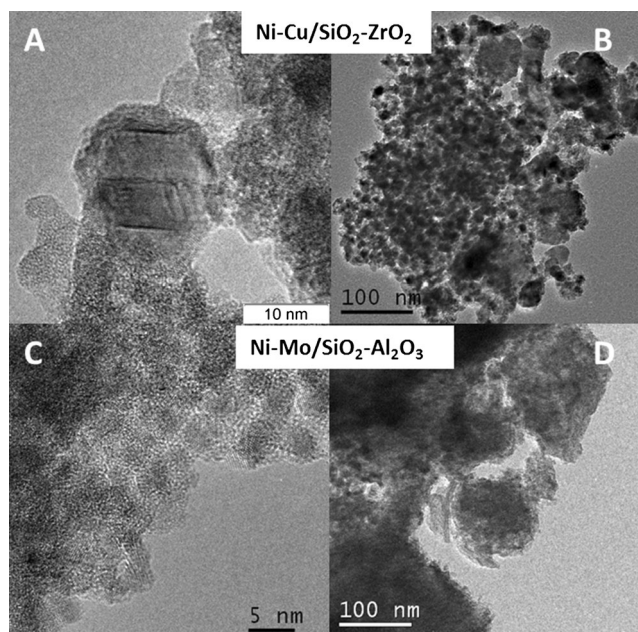


**Fig. 3** TEM images of reduced NiCu/SiO<sub>2</sub>-ZrO<sub>2</sub> (a, b) and NiMo/SiO<sub>2</sub>-Al<sub>2</sub>O<sub>3</sub> (c, d)

SiO<sub>2</sub>-ZrO<sub>2</sub> catalyst closely resembled that of the Ni-Cu catalyst and is not included for brevity.

Images of the reduced bi-metallic catalysts show the presence of well-defined particles of metallic nickel and NiO, in good agreement with the XRD results. In the case of the Ni-Mo catalyst, these particles have sizes of 2–5 nm, which is in good agreement with the CSD sizes obtained by the XRD studies (Table 3).

#### 3.1.4 Ammonia-TPD

The acidity of the three typical catalysts used (Ni/SiO<sub>2</sub>-ZrO<sub>2</sub>, Ni-Cu/SiO<sub>2</sub>-ZrO<sub>2</sub>, and Ni-Mo/SiO<sub>2</sub>-Al<sub>2</sub>O<sub>3</sub>) was investigated by NH<sub>3</sub>-TPD and the results are summarized in Table 4 and Fig. S1 (supporting information).

The acidity of the Ni-Mo/SiO<sub>2</sub>-Al<sub>2</sub>O<sub>3</sub> catalyst (1018 μmol NH<sub>3</sub>/g cat) was the highest in the series and almost twice of that of the other two catalysts. The most plausible explanation for this difference is the matrix for the metal particles, SiO<sub>2</sub>-Al<sub>2</sub>O<sub>3</sub> for the NiMo and SiO<sub>2</sub>-ZrO<sub>2</sub> for the other two catalysts. Acidities of supports are known to vary considerably, but typically the acidity decreases in the order Al<sub>2</sub>O<sub>3</sub> > ZrO<sub>2</sub> > SiO<sub>2</sub> [47]. The differences in acidity in the catalysts used in this study may also affect catalyst performance.

**Table 4** Acidity of Ni/SiO<sub>2</sub>-ZrO<sub>2</sub>, Ni-Cu/SiO<sub>2</sub>-ZrO<sub>2</sub>, and Ni-Mo/SiO<sub>2</sub>-Al<sub>2</sub>O<sub>3</sub> by NH<sub>3</sub>-TPD

Catalyst	μmol NH <sub>3</sub> /g cat
Ni/SiO <sub>2</sub> -ZrO <sub>2</sub>	655
Ni-Cu/SiO <sub>2</sub> -ZrO <sub>2</sub>	557
Ni-Mo/SiO <sub>2</sub> -Al <sub>2</sub> O <sub>3</sub>	1018

## 3.2 Product distribution

Catalytic hydrotreatment reactions were performed using the Ni-based catalysts, either Ni as such (monometallic) or promoted by Cu, Pd, and Mo (bi-metallic) and combinations thereof (tri-metallic). Detailed catalyst compositions are given in Table 2. The catalysts were pre-reduced before reactions. For comparison, experiments were carried out with Ru/C, a benchmark noble metal catalyst. Reactions were performed in a batch set-up at standard conditions (350 °C, 4 h, 140 bar H<sub>2</sub> at the start of the reaction).

The hydrotreatment reactions resulted in the formation of two separate liquid phases, an aqueous and an organic product phase. For Ru/C, Ni-Mo-Cu, and Ni-Mo, the product phase has a density lower than water, while the product appeared as the bottom phase for the other catalysts. The oxygen content in the product oils for the Ni-based catalysts is in a narrow range and between 13.2 and 15.5 wt%. As such, full hydrodeoxygenation at the conditions applied in this study is not taking place, in line with earlier studies using Ni-based catalysts [25, 40]. For Ru/C, the oxygen content is the lowest and actually below 10 wt%. For all liquid product phases, the water content is below 5 wt%, with only minor differences between the catalysts (Table 5).

The amounts of gaseous, organic, aqueous, and solid phases are shown in Table 5. Mass balance closures are >92% for all catalysts. The amounts of organic phases were between 41.5 and 53.1 wt% on feed, whereas the amounts of the aqueous phases were between 35.1 and 42.9 wt% on feed. Solid formation appears very low for all catalysts and is generally below 0.7 wt%. These values are lower than reported in our previous studies on the catalytic hydrotreatment of PLs using Ni-based catalysts (1.2–2.4 wt%) [25, 40] at 350 °C. These differences may be related to the slightly different experimental procedures used in both studies as well as differences in the properties on the PL feeds used (e.g., water content, coking tendency).

The gas phase still contained > 50 mol% of hydrogen, suggesting that the reactions were not carried out under hydrogen starvation conditions. The main gas products are CO<sub>2</sub> and small alkanes (particularly CH<sub>4</sub> and some C<sub>2</sub>-C<sub>3</sub> hydrocarbons). CO<sub>2</sub> is known to be formed by, among others, the decarboxylation of the organic acids in the PL feed and particularly from formic acid [9]. CH<sub>4</sub> is either from gas phase reactions like the methanation of CO<sub>2</sub> and CO [48] or from liquid phase reactions, for instance by gasification of organics [49] and demethoxylation of the lignin fractions in the PL feed [25]. Methanation by gas phase reactions is an undesired reaction as it reduces the carbon efficiency of the process and leads to higher consumption levels of (expensive) hydrogen.

Methane formation appears a strong function of the catalyst composition. For the monometallic Ni and the Pd-promoted catalysts (Ni-Pd and Ni-Pd-Cu), the amount of methane in the



**Table 5** Overview of catalytic hydrotreatment experiments using Ni-based catalysts

Catalysts	Ru/C	Ni monometallic	Ni-Cu	Ni-Pd	Ni-Pd-Cu	Ni-Mo-Cu	Ni-Mo
Organic phase (wt% on PL intake)	41.5	52.7	49.5	52.5	53.1	43.2	42.4
Aqueous phase (wt% on PL intake)	42.9	37.8	38.8	36.0	35.1	40.2	41.5
Solids (wt% on PL intake)	0.1	0.7	0.3	0.1	–	–	0.1
Gas phase (wt% on PL intake)	9.4	5.8	6.7	5.9	5.9	9.8	8.3
Carbon dioxide (mol%)	14.2	8.1	9.0	8.0	7.8	15.6	15.3
Ethane (mol%)	2.5	0.6	1.2	0.7	0.7	4.5	5.4
Propane (mol%)	1.5	0.4	0.8	0.5	0.5	3.0	3.1
Hydrogen (mol%)	54.3	86.9	68.0	84.0	84.8	49.5	56.2
Methane (mol%)	27.5	3.4	20.7	5.5	4.3	27.0	20.0
Carbon monoxide (mol%)	0.0	0.7	0.0	1.3	1.8	0.4	0.0
Mass balance closure (%)	93.9	97.1	95.2	94.4	94.2	93.2	92.4
Hydrogen uptake, NI/kg PL	299	200	276	219	216	317	312
Hydrogen uptake corrected for CH <sub>4</sub> , NI/kg PL	211	187	212	198	201	230	259
Water content of organic phase, wt%	4.4	5.2	4.6	4.7	5.6	2.9	2.9
Elemental composition of organic phase (dry)							
C	81.43	75.86	76.01	75.15	75.81	77.15	77.21
H	9.53	9.08	9.16	9.28	9.27	9.48	9.55
O	9.04	15.06	14.83	15.57	14.92	13.37	13.23
Carbon balance closure, %	89.4	98.8	95.5	98.2	99.4	90.7	88.0
Carbon in gas phase, %	10.2	3.7	6.7	4.2	4.2	11.1	9.1
Carbon in aqueous phase, %	4.7	7.5	6.0	7.1	7.4	4.9	5.3
Carbon in oil phase, %	74.5	87.6	82.8	86.9	87.8	74.7	73.5

gas phase is below 5 mol%. For the Cu- and Mo-promoted catalysts, significantly more methane is present (up to 27 mol% in the gas), close to the Ru/C (27.5 mol%) catalyst, which is a known methanation catalyst [24]. Earlier studies on a Ni-Cu catalyst with a high Ni loading (57.9 wt%) with SiO<sub>2</sub> as the matrix gave by lower rate of methanation (0.2 mol/kg PL) compared to the catalyst used here (2.3 mol/kg PL). The main difference in catalyst composition is the inorganic matrix, viz. SiO<sub>2</sub> versus a SiO<sub>2</sub>-ZrO<sub>2</sub> matrix here. ZrO<sub>2</sub> is known to promote the demethoxylation of the guaiacol and syringol units in the lignin fractions to form CH<sub>4</sub> [25] and this could explain the differences in methanation rates between both catalysts.

The carbon balances for the various catalysts are given in Table 5 and Fig. 4. For this purpose, the elemental composition of the gas and both liquid phases was determined. Carbon balance closures are between 88 and 99%; the lower values for some of the experiments are caused by inaccuracies in weight determination of the organic phase. This is particularly cumbersome in the case a top oil is produced.

Most of the carbon is retained in the organic product phase (>75%), with the highest values for Ni-Pd (>87%). The value for the monometallic Ni catalyst is also in the same range; however, the product properties are not as good as for the Pd-promoted catalysts (vide infra). The organic carbon

recovery in the oil phase using the Mo-promoted catalysts (see Ni-Mo and Ni-Mo-Cu) is around 75%, similar to benchmark Ru/C catalyst. Carbon loss due to the accumulation of organics in the water phase is below 7.5 wt%.

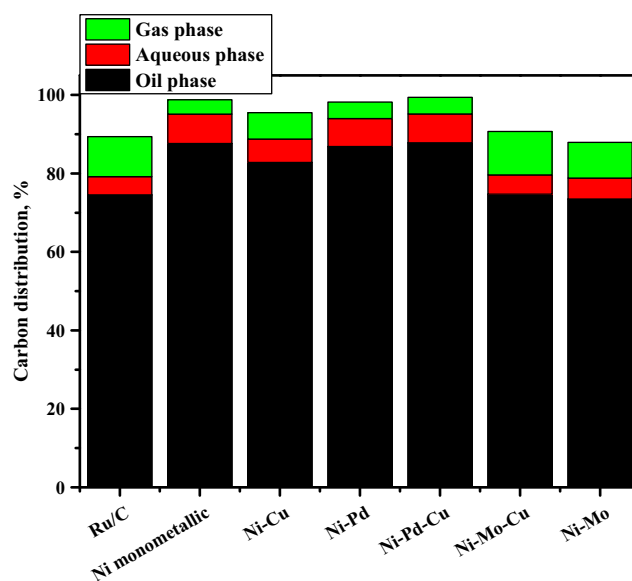


**Fig. 4** Organic carbon distribution for the catalytic hydrotreatment of PLs using Ni-based catalysts and Ru/C at 350 °C for 4 h

### 3.3 Activity of the catalysts

The experimentally determined hydrogen consumption is a good measure for catalytic activity [17, 27]. However, in the case of extensive methane formation, the activity for liquid phase reactions (hydrogenation, hydrodeoxygenation, and hydrocracking) is overestimated when using this procedure. As such, the hydrogen consumption was corrected for methanation reactions (see Section 2 for calculation details) and the results are given in Fig. 5.

The Mo-promoted Ni catalysts show the highest hydrogen consumption (about 260 NL/kg PL feed), whereas the monometallic Ni catalysts is the least active (187 NL/kg PL feed). Thus, Mo addition has a clear positive effect on the activity of the catalysts. The addition of Cu to Ni-based catalysts increases the hydrogen consumption, which is consistent with our previous studies, e.g., hydrogenation of sugar-rich fractions of pyrolysis liquids at 180 °C [50] and whole pyrolysis liquids at 350 °C [25]. Pd addition also has a positive effect on catalysts activity, resulting in higher hydrogen consumptions compared to monometallic Ni catalyst.

### 3.4 Composition of the organic phase

A van Krevelen plot with the elemental composition of the PL feed and the product oils obtained with all catalysts is shown in Fig. 6. The H/C molar ratio of the PL feed is around 1.27, and the values for the product oils using Ni-based catalysts are all higher and in the range of 1.44 to 1.49. The O/C ratio of the product oils is considerably lower (0.10–0.15) than for the PL feed (0.35), though essentially similar for all Ni-based catalysts.

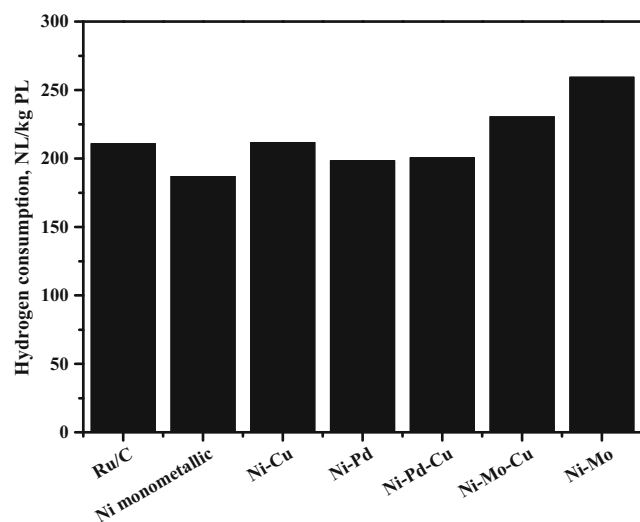


**Fig. 5** Hydrogen consumption (corrected for methane formation) for the Ni-based catalysts and Ru/C

Interestingly, a higher H/C ratio is observed for all oils produced over Ni-based catalysts compared to the benchmark Ru/C catalyst. Higher H/C ratios are indicative for a product with improved product properties such as a higher thermal stability (lower coke formation upon heating). As such, the product oils using the Ni-based catalysts are expected to be preferred compared to those obtained with Ru/C. On a molecular level, it implies that the Ni catalysts are more active hydrogenation catalysts, particularly in the early stage of the reaction than Ru/C.

The H/C ratio for the Ni-based catalysts shows some variations (Fig. 6). The monometallic Ni catalyst yielded a product oil with the lowest H/C ratio among all the Ni-based catalysts. Cu addition to the Ni-based catalysts led to a higher H/C ratio, which is in good agreement with our previous studies on the catalytic hydrotreatment of PLs [25] and sugar fractions thereof [50] using Ni-Cu based catalysts. Pd addition leads to higher H/C ratio in the product oils (see Ni-Pd and Ni-Pd-Cu), likely because Pd is a good hydrogenation catalyst [51].

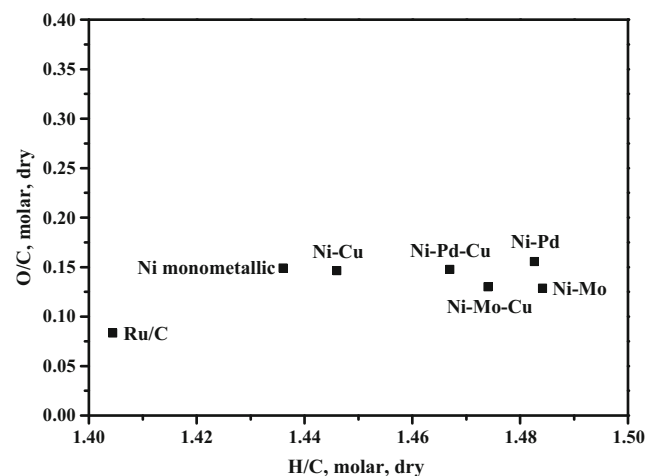
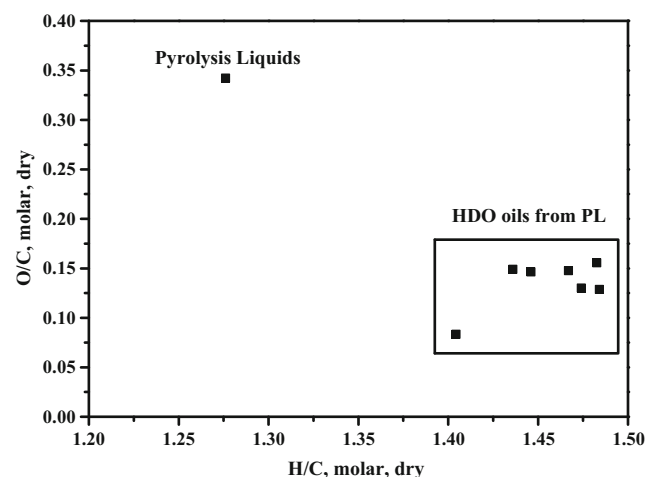


**Fig. 6** van Krevelen plot for the PL feed and products oils after a catalytic hydrotreatment reaction using the Ni-based catalysts and Ru/C (350 °C, 4 h)

The molecular weight distributions of the PL feed and the product oils were analyzed by GPC, and the results are shown in Fig. 7. The crude pyrolysis liquid shows, beside a broad peak extending to a molecular weight of about 3000, a rather sharp peak at a molecular weight around 200 g/mol, which can be attributed (and confirmed by spiking) to levoglucosan (LG). The molecular weight distribution of the PL feed is in line with literature data [52].

The LG peak is considerably lower in the product oils, indicating that LG is converted during the catalytic hydrotreatment [25, 40]. For the product oils, the higher molecular weight tail is significantly reduced to lower values, which indicates that thermal polymerization in the initial stage of the reaction is limited, while hydrocracking at elevated temperatures leads to a reduction of the molecular weight. The molecular tail is shifted to lower molecular weights in particular when using the Mo promoted Ni-based catalysts (Ni-Mo, Ni-Mo-Cu; see Fig. 7 for details). Overall, the molecular weight of the products is much lower than for the original PL feed and this implies that hydrocracking also occurs to a significant extent.

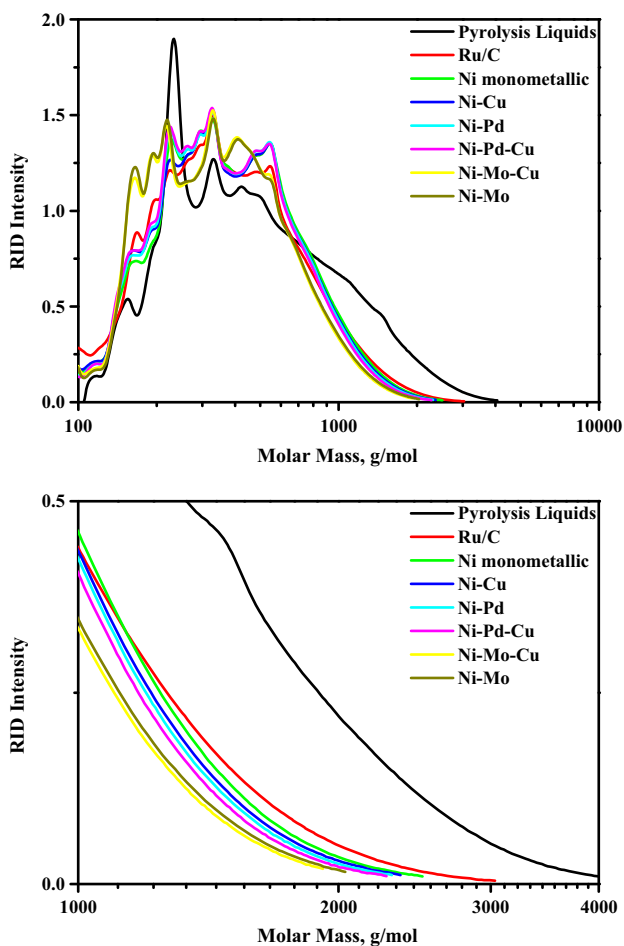


**Fig. 7** Molecular distribution of the PL feed and product oils over nickel-based catalysts and Ru/C by GPC

Charring tendency is known to be another parameter that can be used to qualify product oils from pyrolysis processes [25, 53]. To determine the quality in terms of charring tendency, TGA has shown to be a very suitable method. Specifically the residue (TG residue) after heating the sample in an inert atmosphere till 900 °C is a valuable measure as it actually resembles the MCRT value conventionally used for crude oil feeds [54].

For the PL feed, the TG residue is about 13 wt%, while it is considerably reduced below 3.5 wt% for the product oils as shown in Fig. 8 and Table 6. As such, the catalytic hydrotreatment has led to a considerable improvement in the thermal stability of the oils.

The Mo-promoted catalysts (Ni-Mo and Ni-Mo-Cu) gave the product oils with lowest TG residue (0.7–1.4 wt%), whereas the value was highest with the monometallic Ni and Ni-Cu catalysts (>3 wt%). Thus, to obtain product oils with low TG residues, Mo-promoted Ni catalysts are preferred and show better performance than the Cu- and Pd-promoted catalysts.

### 3.5 Molecular transformations

To investigate the reactions occurring during the catalytic hydrotreatment process, a typical product oil when using the Ni-Mo catalyst and the PL feed was analyzed by  $^1\text{H}$ ,  $^{13}\text{C}$ -NMR, HSQC, and GC  $\times$  GC. The results are shown in Figs. 9, 10, 11, and 12 and Tables 7 and 8.

$^{13}\text{C}$ -NMR spectra and the integration results for the PL feed and the product oil using the Ni-Mo catalyst are shown in Fig. 9 and Table 7. Classification of the various organic groups based on NMR shifts was done using the Ingram method [55].

Clearly, the carbonyl compounds, especially ketones and aldehydes ( $\delta = 163$  to 215 ppm), are readily converted, while carboxylic acids/esters are still present in the product oil in

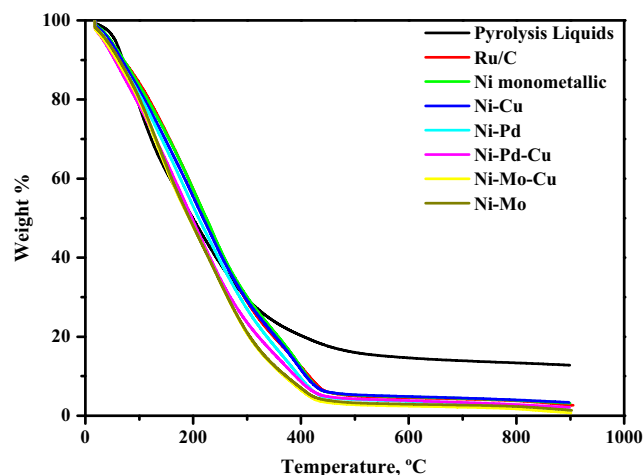


**Fig. 8** TGA data for the PL feed and product oils

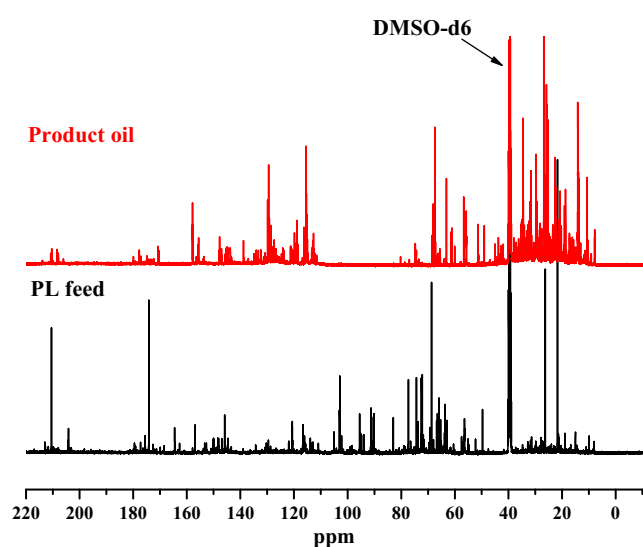
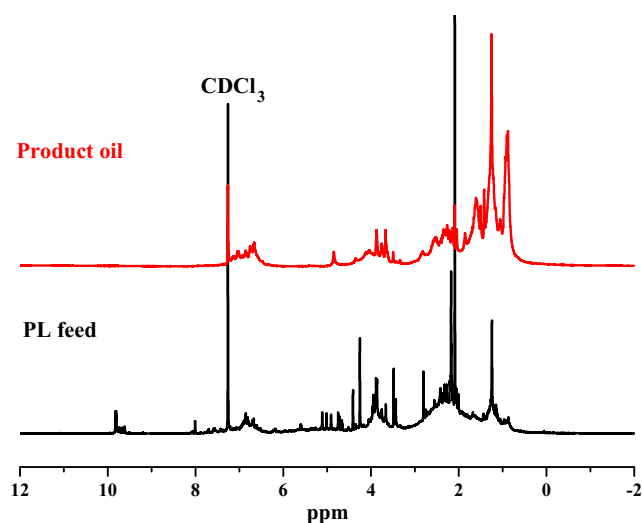
**Table 6** TG residue of PL feed and product oils using the Ni-based catalysts and Ru/C

Catalysts	TG residue, wt% <sup>a</sup>
PL feed	12.8
Ru/C	2.6
Ni monometallic	3.2
Ni-Cu	3.4
Ni-Pd	1.5
Ni-Pd-Cu	2.1
Ni-Mo-Cu	0.7
Ni-Mo	1.4

<sup>a</sup> Defined as the residual weight after heating the sample to 900 °C in an inert atmosphere

considerable amounts. As such, the carboxylic acids/esters are rather inert while the aldehydes and ketones are very reactive. These results are in good agreement with our previous studies on hydrogenated oils using Ni-Cu at different temperatures [40]. The peak intensity of the resonances in the aromatic region, for a larger part arising from the aromatic units of the pyrolytic lignin fraction, decreased from 15.1 in the PL feed to 7.2% in the product oil. As such, the pyrolytic lignin fraction also shows considerable reactivity at the prevailing reaction conditions. Concomitantly, the amount of components with aliphatic carbons increases considerably, as evident from an increase in peak area in the chemical shift range between  $\delta$  1 and 54 ppm.

The resonances between  $\delta$  84 and 110 ppm arising from carbohydrates are clearly present in the PL feed. Upon the hydrotreatment, these peaks disappear, indicative for high reactivity of the carbohydrates at 350 °C.

**Fig. 9** <sup>13</sup>C-NMR spectra of the PL feed and product oil using Ni-Mo at 350 °C for 4 h**Fig. 10** <sup>1</sup>H-NMR spectra of the PL feed and a product oil using Ni-Mo at 350 °C for 4 h

The reactivity of the various organic component classes in the PLs was also confirmed by <sup>1</sup>H-NMR measurements. The percentages of protons of various groups in the product oils and PL feed were classified using a reported procedure by Mullen et al. [56] (see Fig. 10 and Table 8 for details).

Aldehydes with typical resonances in the chemical shift region from  $\delta$  8.0 to 10.0 ppm are fully converted. In addition, the peak intensity of resonances arising from carbohydrates ( $\delta$  4.2–6.4 ppm) is also reduced considerably, indicative for a high reactivity of this fraction. The main products are aliphatics with resonances in the range between  $\delta$  0.0 and 1.6 ppm.

Extensively used for lignin characterization, we also analyzed the liquid product samples using <sup>1</sup>H-<sup>13</sup>C HSQC [57]. The overlay of spectra for the crude PL feed and a typical product oil using the Ni-Mo catalyst is given in Fig. 11.

The results supplement the separate <sup>1</sup>H and <sup>13</sup>C-NMR measurements. For instance, it shows that –OMe groups on aromatic rings present in the lignin fraction are partly converted. In addition, major individual components can be clearly identified, the most prominent example being LG. Characteristic resonances of LG in the PL feed (Fig. 11) are absent in the product oil, indicative for quantitative conversion.

The high reactivity of aldehydes, ketones, and carbohydrates as observed by NMR techniques is further confirmed by GC  $\times$  GC measurements as shown in Fig. 12. The amounts of phenolics, alcohols, methoxyphenolics, and hydrocarbons increased to a certain extent at the expense of sugars, aldehydes, and ketones. The phenolics and methoxyphenolics likely arise from the hydrocracking of the pyrolytic lignin fraction. Considerable amounts of carboxylic acids are still present in the product oil, confirming their rather inert nature. The GC  $\times$  GC results are consistent with the NMR results provided in Figs. 9, 10, and 11.

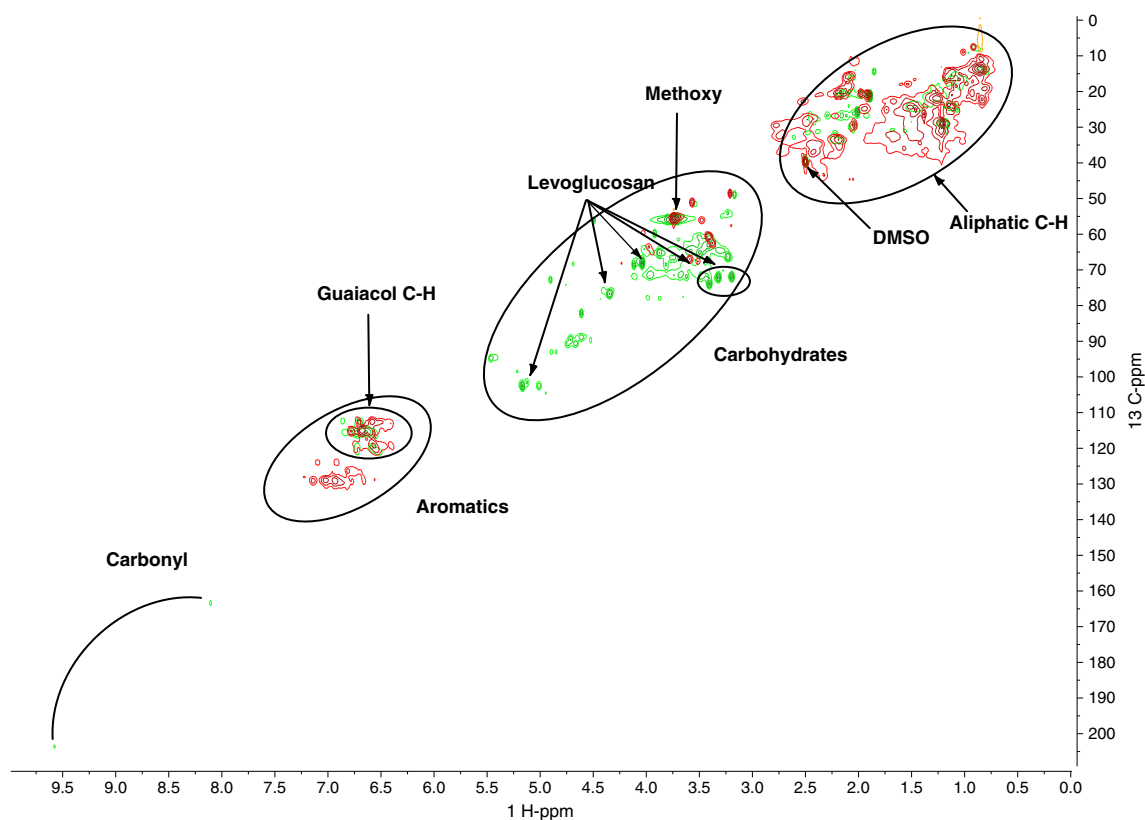


**Fig. 11** Heteronuclear single quantum coherence (HSQC) spectra of the PL feed (*green*) and product oil (*red*) after a catalytic hydrotreatment over Ni-Mo at 350 °C for 4 h

### 3.6 Catalyst selection

Suitable catalysts for the catalytic hydrotreatment lead to organic products with favorable product properties such as low charring tendency (low TG residue) and a high H/C ratio. In addition, the carbon is preferably retained quantitatively in the organic product phase. A high H/C ratio generally corresponds with a higher energy density of the product oil. Furthermore, it is known to lead to improved solubility in apolar solvents, which is advantageous when considering co-feeding of the product in FCC refinery units. A plot with

the three relevant quality indicators as a function of the catalyst composition is given in Fig. 13. The preferred catalysts are in the right bottom of part the graph.

Based on this figure, the preferred catalysts regarding product properties are the Mo-promoted catalysts and the Ni-Pd catalyst. When also taking into account the carbon balance, the Pd-based catalysts (Ni-Pd and Ni-Pd-Cu) seem preferred (Fig. 13). However, when considering that Pd is around 1350 times more expensive than Mo (22,000 US\$/kg for Pd versus 16.3 US\$/kg for Mo [58]), Mo can be considered a good promoter for these Ni-

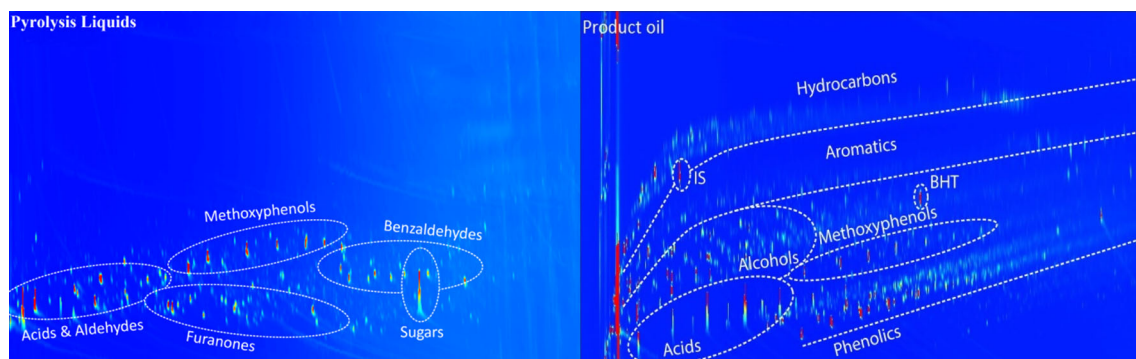


**Fig. 12** GC × GC spectrum of the PL feed and product oil using Ni-Mo at 350 °C for 4 h (IS is the internal standard, BHT is the stabilizer in THF)

**Table 7**  $^{13}\text{C}$ -NMR data for the PL feed and a product oil from a reaction with Ni-Mo at 350 °C for 4 h

Chemical shift region $\delta$ (ppm)	Carbon assignments	PL feed (%-C)	Product oil Ni-Mo (%-C)
215–163	Total carbonyl	6.7	1.8
215–180	Carbonyl (ketones + aldehydes)	3.8	0.5
180–163	Carbonyl (esters + carboxylic acids)	2.9	1.3
163–100	Total aromatics	15.1	7.2
163–125	General aromatics	5.6	4.2
125–112	Aromatics (guaiacyl)	7.1	2.9
112–100	Aromatics (syringyl)	2.4	0.1
110–84	Carbohydrates	2.8	0.0
84–54	Methoxy/hydroxyl groups	20.1	2.0
54–1	Alkyl carbon (total)	16.8	40.1
54–36	Long/branched aliphatics	0.1	3.1
36–1	Short aliphatics	16.7	36.9

based catalysts. This price difference is of particular relevance when irreversible catalyst deactivation plays a role, which needs to be established by detailed catalyst stability studies in continuous set-ups.

Despite these positive effects of Mo promotion, catalyst improvements are required in terms of the organic carbon yields, which are lower for the Mo-promoted catalysts compared to the Pd-promoted ones. The main difference between Pd- and Mo-promoted catalysts when considering the carbon distribution over the product phases is a higher amount of methane in the gas phase for Mo. Methane is to a large extent formed by gas phase reactions of CO and CO<sub>2</sub>. As such, catalyst modification studies to reduce the decarboxylation activity as well as the rate of subsequent gas phase reactions to methane should be a major topic for future catalyst development for noble metal free Ni-based catalysts.

Performance of the benchmark Ru/C catalyst is worse than for the Ni-based catalysts particularly when considering the product properties. For the monometallic Ni and bi-metallic Ni-Cu catalysts, the product properties are also by far worse than for Mo-promoted catalysts.

The good performance of the Ni-Mo catalyst may be related to the presence of relatively small particles (5 nm, TEM and XRD), which at least partly consist of a NiMo solid solution (30%, Table 3). These bi-metallic particles may be more active than monometallic ones and may explain the higher activity of the NiMo catalyst compared to the monometallic ones. In addition, when structure sensitivity plays a role, the smaller Ni particles for the bimetallic Ni-Mo catalyst compared to the Ni-Cu and monometallic Ni catalysts may be more active than the larger ones. However, it is also well possible that Mo in intermediate oxidation states have (in combination with Ni) a positive effect on activity by activation of oxygenated species. Evidence for the latter has been reported for the hydrodeoxygenation of esters using Mo-supported Ni catalysts [59]. In addition, the high acidity of the support compared to the monometallic Ni and bimetallic Ni-Cu may also play a role and affect the performance of the catalyst.

Of interest is the observation that significant amounts of oxidized Ni species are still present in the in situ reduced NiMo catalyst (Table 3). When assuming that reduced species are more active, further studies using higher reduction

**Table 8**  $^1\text{H}$ -NMR data for pyrolysis liquids feed and product oils using Ni-Mo at 350 °C for 4 h

Chemical shift region $\delta$ (ppm)	Proton assignments	PL feed (%-H)	Product oil Ni-Mo (%-H)
10.0–8.0	–CHO, –COOH, downfield ArH	1.7	0
8.0–6.8	ArH, HC=C (conjugated)	4.9	4.2
6.8–6.4	HC=C (nonconjugated)	2.8	3.8
6.4–4.2	–CH <sub>n</sub> –O–, ArOH, HC=C (nonconjugated)	12.1	3.2
4.2–3.0	CH <sub>3</sub> O–, –CH <sub>2</sub> O–, –CHO–	17.1	9.9
3.0–2.2	CH <sub>3</sub> (=O)–, CH <sub>3</sub> -Ar, –CH <sub>2</sub> Ar	22.2	13.9
2.2–1.6	–CH <sub>2</sub> –, aliphatic OH	21.5	15.1
1.6–0.0	–CH <sub>3</sub> , –CH <sub>2</sub> –	17.6	49.9

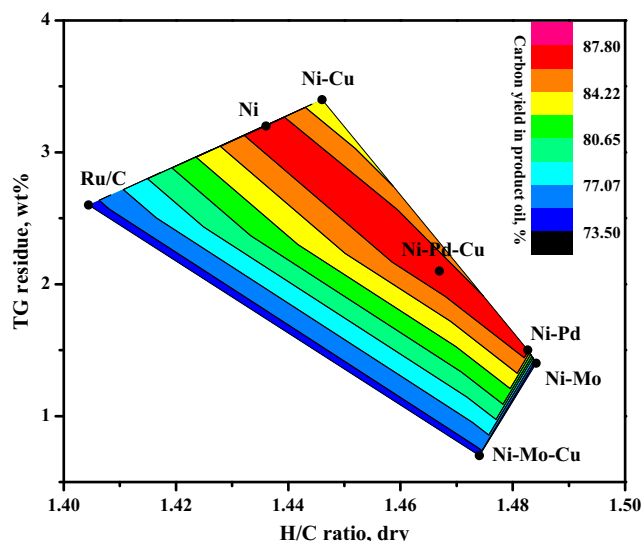


**Fig. 13** Quality indicators (TG residue, H/C ratio, carbon yield in product phase) for the Ni-based catalysts and Ru/C

temperatures may be advantageous when considering catalyst activity. These studies are beyond the scope of the current paper.

## 4 Conclusions

The catalytic hydrotreatment of PLs using nickel-based catalysts promoted by Cu, Pd, and Mo was investigated at 350 °C. Best performance on basis of H/C ratio (dry product based) and TG residue was obtained by promotion with Mo. For these catalysts, the reaction rate, expressed as the hydrogen uptake corrected for methane formation per kilogram PL feed, was also the highest. Carbon balance calculations show that the amount of carbon ending up in the organic product phase is actually higher for Pd (85%) than for Mo promotion (75%) due to a higher methanation activity of the Mo-promoted catalysts. The actual rate of methanation of the Ni-Mo catalyst is similar to the benchmark Ru/C. Further catalyst studies should be aimed to prepare catalysts with reduced methanation activity. Analysis of the product oil ( $^1\text{H}$ ,  $^{13}\text{C}$ -NMR, HSQC, and GC  $\times$  GC) obtained with the Ni-Mo catalyst revealed that aldehydes, ketones, and carbohydrates are readily converted, while the pyrolytic lignin fraction is more inert, though prone to hydrocracking (GPC).

**Acknowledgements** Financial support from Agentschap NL (Groene aardolie via pyrolyse, GAP) is gratefully acknowledged. The authors thank Arjan Kloekhorst and Monique Bernardes Figueirêdo (Department of Chemical Engineering, University of Groningen) for NMR analysis. Hans van der Velde (Stratingh Institute for Chemistry, University of Groningen) is acknowledged for performing the elemental analyses and G. O. R. Alberda van Ekenstein (Department of Polymer Chemistry, Zernike Institute for Advanced Materials, University of Groningen) for TGA analysis. We also thank Leon Rohrbach, Jan Henk Marsman Erwin Wilbers, Marcel de Vries, and Anne Appeldoorn

(Department of Chemical Engineering, ENTEG, University of Groningen) for analytical and technical support.

**Open Access** This article is distributed under the terms of the Creative Commons Attribution 4.0 International License (<http://creativecommons.org/licenses/by/4.0/>), which permits unrestricted use, distribution, and reproduction in any medium, provided you give appropriate credit to the original author(s) and the source, provide a link to the Creative Commons license, and indicate if changes were made.

## References

- Chheda JN, Huber GW, Dumesic JA (2007) Liquid-phase catalytic processing of biomass-derived oxygenated hydrocarbons to fuels and chemicals. *Angew Chem Int Ed Engl* 46(38):7164–7183
- Venderbosch RH, Ardiyanti AR, Wildschut J, Oasmaa A, Heeres HJ (2010) Stabilization of biomass-derived pyrolysis oils. *J Chem Technol Biotechnol* 85(5):674–686
- Venderbosch R, Prins W (2010) Fast pyrolysis technology development. *Biofuels Bioprod Biorefin* 4(2):178–208
- Oasmaa A, Kuoppala E, Ardiyanti A, Venderbosch RH, Heeres HJ (2010) Characterization of hydrotreated fast pyrolysis liquids. *Energy Fuel* 24(9):5264–5272
- Oasmaa A, Elliott DC, Korhonen J (2010) Acidity of biomass fast pyrolysis bio-oils. *Energy Fuel* 24(12):6548–6554
- Oasmaa A, Kuoppala E, Elliott DC (2012) Development of the basis for an analytical protocol for feeds and products of bio-oil hydrotreatment. *Energy Fuel* 26(4):2454–2460
- Oasmaa A, Korhonen J, Kuoppala E (2011) An approach for stability measurement of wood-based fast pyrolysis bio-oils. *Energy Fuel* 25(7):3307–3313
- Wang H, Male J, Wang Y (2013) Recent advances in hydrotreating of pyrolysis bio-oil and its oxygen-containing model compounds. *ACS Catal* 3(5):1047–1070
- Zacher AH, Olarte MV, Santosa DM, Elliott DC, Jones SB (2014) A review and perspective of recent bio-oil hydrotreating research. *Green Chem* 45(12):491–515
- Elliott DC (2007) Historical developments in hydroprocessing bio-oils. *Energy Fuel* 21(3):1792–1815
- Mercader FM, Groeneveld MJ, Kersten SRA, Venderbosch RH, Hogendoorn JA (2010) Pyrolysis oil upgrading by high pressure thermal treatment. *Fuel* 89(10):2829–2837
- Mortensen PM, Grunwaldt JD, Jensen PA, Knudsen KG, Jensen AD (2011) A review of catalytic upgrading of bio-oil to engine fuels. *Appl Catal A Gen* 407(1–2):1–19
- Elliott DC, Hart TR, Neuenschwander GG, Rotness LJ, Olarte MV, Zacher AH, Solantausta Y (2012) Catalytic hydroprocessing of fast pyrolysis bio-oil from pine sawdust. *Energy Fuel* 26(6):3891–3896
- Elliott DC, Hart TR (2009) Catalytic hydroprocessing of chemical models for bio-oil. *Energy Fuel* 23(2):631–637
- Wildschut J, Mahfud FH, Venderbosch RH, Heeres HJ (2009) Hydrotreatment of fast pyrolysis oil using heterogeneous noble-metal catalysts. *Ind Eng Chem Res* 48(23):10324–10334
- Baldauf W, Balfanz U, Rupp M (1994) Upgrading of flash pyrolysis oil and utilization in refineries. *Biomass Bioenergy* 7(1):237–244
- Ardiyanti AR, Gutierrez A, Honkela ML, Krause AOI, Heeres HJ (2011) Hydrotreatment of wood-based pyrolysis oil using zirconia-supported mono- and bimetallic (Pt, Pd, Rh) catalysts. *Appl Catal A Gen* 407(1–2):56–66
- Wang WY, Yang YQ, Bao JG, Chen Z (2009) Influence of ultrasonic on the preparation of Ni–Mo–B amorphous catalyst and its performance in phenol hydrodeoxygenation. *J Fuel Chem Technol* 37(6):701–706

19. Wang W, Yang Y, Luo H, Hu T, Liu W (2011) Amorphous Co–Mo–B catalyst with high activity for the hydrodeoxygenation of bio-oil. *Catal Commun* 12(6):436–440
20. Wang W, Yang Y, Luo H, Peng H, Wang F (2011) Effect of La on Ni–W–B amorphous catalysts in hydrodeoxygenation of phenol. *Ind Eng Chem Res* 50(19):10936–10942
21. Wang W, Yang Y, Luo H, Peng H, He B, Liu W (2011) Preparation of Ni(Co)–W–B amorphous catalysts for cyclopentanone hydrodeoxygenation. *Catal Commun* 12(14):1275–1279
22. Zhao HY, Li D, Bui P, Oyama ST (2011) Hydrodeoxygenation of guaiacol as model compound for pyrolysis oil on transition metal phosphide hydroprocessing catalysts. *Appl Catal A Gen* 391(1–2):305–310
23. Ardiyanti AR, Khromova SA, Venderbosch RH, Yakovlev VA, Heeres HJ (2012) Catalytic hydrotreatment of fast-pyrolysis oil using non-sulfided bimetallic Ni–Cu catalysts on a  $\delta$ -Al<sub>2</sub>O<sub>3</sub> support. *Appl Catal B Environ* 117–118:105–117
24. Ardiyanti AR (2013) Hydrotreatment of fast pyrolysis oil: catalyst development and process-product relations. Ph.D Thesis. University of Groningen, Groningen
25. Ardiyanti AR, Bykova MV, Khromova SA, Yin W, Venderbosch RH, Yakovlev VA, Heeres HJ (2016) Ni-based catalysts for the hydrotreatment of fast pyrolysis oil. *Energy Fuel* 30(3):1544–1554
26. Wildschut J, Iqbal M, Mahfud FH, Cabrera IM, Venderbosch RH, Heeres HJ (2010) Insights in the hydrotreatment of fast pyrolysis oil using a ruthenium on carbon catalyst. *Energy Environ Sci* 3(7):962
27. Ardiyanti AR, Khromova SA, Venderbosch RH, Yakovlev VA, Melián-Cabrera IV, Heeres HJ (2012) Catalytic hydrotreatment of fast pyrolysis oil using bimetallic Ni–Cu catalysts on various supports. *Appl Catal A: Gen* 449:121–130
28. Wildschut J, Melián-Cabrera I, Heeres HJ (2010) Catalyst studies on the hydrotreatment of fast pyrolysis oil. *Appl Catal B Environ* 99(1–2):298–306
29. Bykova MV, Ermakov DY, Kaichev VV, Bulavchenko OA, Saraev AA, Lebedev MY, Yakovlev VA (2012) Ni-based sol–gel catalysts as promising systems for crude bio-oil upgrading: guaiacol hydrodeoxygenation study. *Appl Catal B Environ* 113–114:296–307
30. Bykova MV, Ermakov DY, Khromova SA, Smirnov AA, Lebedev MY, Yakovlev VA (2014) Stabilized Ni-based catalysts for bio-oil hydrotreatment: reactivity studies using guaiacol. *Catal Today* 220–222:21–31
31. Yakovlev VA, Bykova MV, Khromova SA (2012) Stability of nickel-containing catalysts for hydrodeoxygenation of biomass pyrolysis products. *Catal Ind* 4(4):324–339
32. Yakovlev VA, Khromova SA, Sherstyuk OV, Dundich VO, Ermakov DY, Novopashina VM, Lebedev MY, Bulavchenko O, Parmon VN (2009) Development of new catalytic systems for upgraded bio-fuels production from bio-crude-oil and biodiesel. *Catal Today* 144(3–4):362–366
33. Kloekhorst A, Heeres HJ (2015) Catalytic Hydrotreatment of Alcell lignin using supported Ru, Pd, and Cu catalysts. *ACS Sustain Chem Eng* 3(9):1905–1914
34. Kloekhorst A, Wildschut J, Heeres HJ (2014) Catalytic hydrotreatment of pyrolytic lignins to give alkylphenolics and aromatics using a supported Ru catalyst. *Catal Sci Technol* 4(8):2367–2377
35. Kumar CR, Anand N, Kloekhorst A, Cannilla C, Bonura G, Frusteri F, Barta K, Heeres HJ (2015) Solvent free depolymerization of Kraft lignin to alkyl-phenolics using supported NiMo and CoMo catalysts. *Green Chem* 17(11):4921–4930
36. Bykova MV, Bulavchenko OA, Ermakov DY, Lebedev MY, Yakovlev VA, Parmon VN (2011) Guaiacol hydrodeoxygenation in the presence of Ni-containing catalysts. *Catal Ind* 3(1):15–22
37. Ermakova MA, Ermakov DY (2003) High-loaded nickel–silica catalysts for hydrogenation, prepared by sol–gel: route: structure and catalytic behavior. *Appl Catal A Gen* 245(245):277–288
38. Popa T, Zhang Y, Jin E, Fan M (2015) An environmentally benign and low-cost approach to synthesis of thermally stable industrial catalyst Cu/SiO<sub>2</sub> for the hydrogenation of dimethyl oxalate to ethylene glycol. *Appl Catal A Gen* 505(2):52–61
39. Mile B, Stirling D, Zammit MA, Lovell A, Webb M (1988) ChemInform abstract: location of nickel oxide and nickel in silica-supported catalysts: two forms of “NiO” and the assignment of temperature-programmed reduction profiles. *J Catal* 114(2):217–229
40. Yin W, Kloekhorst A, Venderbosch RH, Bykova MV, Khromova SA, Yakovlev VA, Heeres HJ (2016) Catalytic hydrotreatment of fast pyrolysis liquids in batch and continuous set-ups using a bimetallic Ni–Cu catalyst with a high metal content. *Catal Sci Technol* 6(15):5899–5915
41. Scherrer P (1918) *Nachr. Ges. Wiss. Göttingen* 2:96–100
42. Rietveld HM (1969) A profile refinement method for nuclear and magnetic structures. *J Appl Crystallogr* 2(2):65–71
43. Mortensen PM, Grunwaldt J-D, Jensen PA, Jensen AD (2016) Influence on nickel particle size on the hydrodeoxygenation of phenol over Ni/SiO<sub>2</sub>. *Catal Today* 259:277–284
44. He J, Zhao C, Lercher JA (2012) Ni-catalyzed cleavage of aryl ethers in the aqueous phase. *J Am Chem Soc* 134(51):20768–20775
45. Van Santen RA (2008) Complementary structure sensitive and insensitive catalytic relationships. *Acc Chem Res* 42:57–66
46. Murzin DY (2010) Kinetic analysis of cluster size dependent activity and selectivity. *J Catal* 276(1):85–91
47. Wu SK, Lai PC, Lin YC, Wan HP, Lee HT, Chang YH (2013) Atmospheric hydrodeoxygenation of guaiacol over alumina-, zirconia-, and silica-supported nickel phosphide catalysts. *ACS Sustain Chem Eng* 1(3):349–358
48. Navalikhina MD, Krylov OV (1998) Heterogeneous hydrogenation catalysts. *Russ Chem Rev* 67:587–616
49. Trane-Restrup R, Jensen AD (2015) Steam reforming of cyclic model compounds of bio-oil over Ni-based catalysts: product distribution and carbon formation. *Appl Catal B Environ* 165:117–127
50. Yin W, Venderbosch RH, Bykova MV, Heeres H, Khromova SA, Yakovlev VA, Cannilla C, Bonura G, Frusteri F, Heeres HJ (2016) Hydrotreatment of the carbohydrate fraction of pyrolysis liquids using bimetallic Ni based catalyst: catalyst activity and product property relations. Submitted
51. Elliott DC, Hu J, Hart TR, Neuenschwander GG (2008) Palladium catalyzed hydrogenation of bio-oils and organic compounds, Patent International, 7425657
52. Hoekstra E, Kersten SRA, Tudos A, Meier D, Hogendoorn KJA (2011) Possibilities and pitfalls in analyzing (upgraded) pyrolysis oil by size exclusion chromatography (SEC). *J Anal Appl Pyrolysis* 91(1):76–88
53. de Miguel MF, Groeneveld MJ, Kersten SRA, Geantet C, Toussaint G, Way NWJ, Schaverien CJ, Hogendoorn KJA (2011) Hydrodeoxygenation of pyrolysis oil fractions: process understanding and quality assessment through co-processing in refinery units. *Energy Environ Sci* 4(3):985
54. Ghetti P (1994) A rapid heating TGA method for evaluating the carbon residue of fuel oil. *Fuel* 73(12):1918–1921
55. Ingram L, Mohan D, Bricka M, Steele P, Strobel D, Crocker D, Mitchell B, Mohammad J, Cantrell K, Jr CUP (2008) Pyrolysis of wood and bark in an auger reactor: physical properties and chemical analysis of the produced bio-oils. *Energy Fuel* 22(22):614–625
56. Mullen CA, Strahan GD, Boateng AA (2009) Characterization of various fast-pyrolysis bio-oils by NMR spectroscopy†. *Energy Fuel* 23(5):2707–2718
57. Kloekhorst A, Heeres E (2016) Catalytic hydrotreatment of Alcell lignin fractions using a Ru/C catalyst. *Catal Sci Technol* 6(19):7053–7067
58. London metal exchange, [www.lme.com](http://www.lme.com) (accessed Sept 2016)
59. Kukushkin RG, Bulavchenko OA, Kaichev VV, Yakovlev VA (2015) Influence of Mo on catalytic activity of Ni-based catalysts in hydrodeoxygenation of esters. *Appl Catal B Environ* 163:531–538